

TurboVGGT: Fast Visual Geometry Reconstruction with Adaptive Alternating Attention

David Huang^{1,2,*,†} Guile Wu^{1,†} Chengjie Huang¹ Bingbing Liu³ Dongfeng Bai¹
¹Huawei Noah’s Ark Lab ²University of Toronto ³Foundation Model Department, Huawei
 dawae.huang@mail.utoronto.ca, {guile.wu, chengjie.huang}@outlook.com,
 {baidongfeng, liu.bingbing}@huawei.com

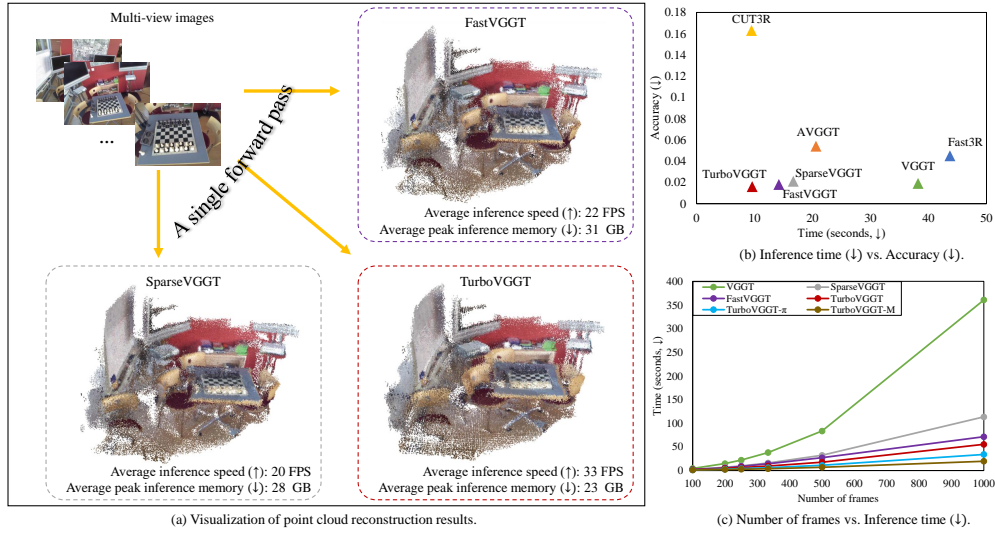


Figure 1: An illustration of our TurboVGGT for fast multi-view 3D reconstruction. (a) Visualization of point cloud reconstruction results. TurboVGGT significantly improves computational efficiency in terms of inference time and peak GPU memory usage. (b) Comparison of inference time vs. point cloud accuracy on 7-Scenes. TurboVGGT achieves a better trade-off between accuracy and efficiency compared to state-of-the-art methods. (c) Comparison of number of frames vs. inference time on 7-Scenes. TurboVGGT scales more efficiently with the number of input frames. TurboVGGT/TurboVGGT- π /TurboVGGT-M achieve $7\times/11\times/18\times$ speedup compared to VGGT for processing input sequences of 1000 frames.

ABSTRACT

Recent feed-forward 3D reconstruction methods, such as visual geometry transformers, have substantially advanced the traditional per-scene optimization paradigm by enabling effective multi-view reconstruction in a single forward pass. However, most existing methods struggle to achieve a balance between reconstruction quality and computational efficiency, which limits their scalability and efficiency. Although some efficient visual geometry transformers have recently emerged, they typically use the same sparsity ratio across layers and frames and lack mechanisms to adaptively learn representative tokens to capture global relationships, leading to suboptimal performance. In this work, we propose TurboVGGT, a novel approach that employs an efficient visual geometry transformer with adaptive alternating attention for fast multi-view 3D reconstruction. Specifically, TurboVGGT employs an end-to-end trainable framework with adaptive sparse global attention

*David Huang contributed to this work during an internship at Huawei Canada.

†Equal contribution.

guided by adaptive sparsity selection to capture global relationships across frames and frame attention to aggregate local details within each frame. In the adaptive sparse global attention, TurboVGGT adaptively learns representative tokens with varying sparsity levels for global geometry modeling, considering that token importance varies across frames, attention layers operate tokens at different levels of abstraction, and global dependencies rely on structurally informative regions. Extensive experiments on multiple 3D reconstruction benchmarks demonstrate that TurboVGGT achieves fast multi-view reconstruction while maintaining competitive reconstruction quality compared with state-of-the-art methods. Project page: <https://turbovgg.t.github.io/>.

1 Introduction

Multi-view 3D reconstruction is a long-standing problem in computer vision. It aims to reconstruct the 3D geometry of a scene from a set of 2D images captured from different views. It has been widely used in various applications, such as robotics, autonomous driving, and virtual reality. Traditional methods, such as Structure-from-Motion (SfM) [31] and Multi-View Stereo (MVS) [32], typically employ a multi-stage paradigm to estimate camera poses and reconstruct 3D geometry. This paradigm is effective in producing accurate reconstructions but suffers from high computational costs.

Recently, learning-based 3D reconstruction [41, 39, 40, 20] has emerged as a promising alternative to the traditional paradigm, shifting from per-scene iterative optimization to direct inference of 3D geometry from images using end-to-end neural networks. In particular, the emergence of visual geometry transformer based feed-forward reconstruction methods, such as VGGT [39], MapAnything [20], and π^3 [43], have revolutionized multi-view 3D reconstruction, enabling efficient and robust estimation of camera poses, depth maps, and point maps in a single forward pass. Despite the significant progress, these methods still face challenges in achieving a balance between reconstruction quality and computational efficiency. This limits their scalability and hinders their application in time-sensitive scenarios. More recently, several studies [33, 44, 35, 38] have revealed that the high computational cost of visual geometry transformers primarily lies in the dense global token interactions within global attention layers, which involve quadratic complexity with respect to the number of input tokens. To resolve this problem, existing methods typically use token merging, sparse attention or token subsampling strategies to reduce the number of tokens involved in the global attention. Although these methods can accelerate visual geometry transformers for 3D reconstruction, they still have some limitations. First, they typically employ the same sparsity ratio across layers and frames. This may be suboptimal because token importance can vary across frames and attention layers operate tokens at different levels of abstraction. Second, they lack mechanisms to adaptively learn representative tokens that can effectively capture global relationships. Since global dependencies often rely on structurally informative regions, learning representative tokens can facilitate global geometry modeling and reduce redundant computations.

To address these limitations, in this work, we propose a novel approach named TurboVGGT, which improves the efficiency of visual geometry transformers for fast multi-view 3D reconstruction. The key idea of TurboVGGT is to construct a visual geometry transformer with adaptive alternating attention blocks, which consists of adaptive sparse global attention guided by adaptive sparsity selection to capture global relationships and frame attention to aggregate local details within each frame. Specifically, considering that token importance can vary across frames and attention layers operate tokens at different levels of abstraction, TurboVGGT employs a gating network to adaptively assign different sparsity ratios for different frames across global attention layers. Then, in each branch corresponding to a specific sparsity level, TurboVGGT employs adaptive sparse global attention to learn compressed representative tokens for global geometry modeling. This enables TurboVGGT to effectively learn representative tokens to capture global relationships while reducing redundant computations. In addition, following existing works [39], TurboVGGT also incorporates frame attention to aggregate local details within each frame. We conduct extensive experiments on multiple 3D reconstruction benchmarks to evaluate the proposed TurboVGGT. Experimental results demonstrate the superiority of TurboVGGT over state-of-the-art methods in achieving fast multi-view 3D reconstruction while maintaining high reconstruction quality (as illustrated in Figure 1).

In summary, our **contributions** are:

- We present a novel visual geometry transformer with adaptive alternating attention blocks for fast multi-view 3D reconstruction.
- We propose an adaptive sparsity selection mechanism for visual geometry transformers, which adaptively selects different sparsity ratios for different frames across different layers.
- We propose adaptive sparse global attention for visual geometry transformers, which learns representative tokens to model global geometry relationships.
- We conduct extensive experiments on multiple 3D reconstruction benchmarks and demonstrate the superiority of the proposed approach over state-of-the-art methods.

2 Related Work

2.1 Multi-View 3D Reconstruction

Reconstructing 3D scenes from multi-view images is a fundamental problem in computer vision. The traditional paradigm consists of multiple stages, such as feature extraction and matching, camera pose estimation, triangulation, and bundle adjustment. Typically, Structure-from-Motion [31, 28] is employed to estimate camera parameters and reconstruct sparse point clouds from multi-view images, and Multi-View Stereo [32, 12] is used to reconstruct dense geometry of 3D scenes. Although these methods can achieve high-quality reconstruction, they rely on per-scene iterative optimization, which is computationally expensive and time-consuming. Recently, learning-based methods have been proposed to directly predict 3D geometry from multi-view images in end-to-end neural networks [41, 39, 21, 20, 46, 43]. DUST3R [41] is a pioneering work that employs transformer networks to directly predict dense 3D geometry from image pairs, but it requires costly global alignment when extending to large scenes due to the reliance on pairwise view processing. Subsequent works, such as MAST3R [21], CUT3R [40], Fast3R [46], DDUST3R [14], and VGGT [39], have presented various strategies to resolve the limitations of DUST3R for different problem settings, such as large scenes, long sequences, and dynamic scenes. Our work belongs to the learning-based paradigm, and we focus on improving the efficiency of visual geometry transformers for fast multi-view 3D reconstruction, which is a critical problem but has not been well explored in existing works.

2.2 Visual Geometry Transformers

Visual geometry transformers [39, 20, 43, 54] have recently emerged as powerful models for feed-forward multi-view 3D reconstruction. They can directly predict camera intrinsics, camera extrinsics, depth maps, point maps, and other geometric properties from multi-view images in a single forward pass. VGGT [39] is a pioneering work that constructs a visual geometry transformer and optimizes it with multi-task learning and large-scale datasets. π^3 [43] is a subsequent work that introduces a fully permutation-equivariant architecture to eliminate the reliance on a fixed reference view in VGGT. MapAnything [20] proposes a unified feed-forward transformer that supports various problem settings with different input and output configurations. Despite their impressive performance, they still face challenges in computational efficiency. This limits their scalability and efficiency in time-sensitive application scenarios. Although there have been some recent efforts [33, 44, 35, 38] to accelerate visual geometry transformers, they still have some limitations, such as relying on a fixed sparsity ratio for all layers and frames and lacking mechanisms to adaptively learn representative tokens for global geometry modeling. To address these limitations, our work proposes a novel visual geometry transformer with adaptive alternating attention blocks, which can adaptively select different sparsity ratios for different frames and learn representative tokens to model global geometry while reducing redundant computations, thus improving the efficiency of feed-forward 3D reconstruction.

2.3 Efficient Vision Transformers

Vision transformers [10] have achieved incredible success in computer vision. To make vision transformers more efficient, various strategies have been used, such as FlashAttention [9, 8], sparse attention [45, 50], token merging [4, 49], and low-rank approximation [17, 13]. Despite their efficiency, most efficient vision transformers are designed for general 2D vision tasks. In the context of multi-view 3D reconstruction, designing an efficient visual transformer remains an open question, as it requires modeling complex global geometric relationships across views and local

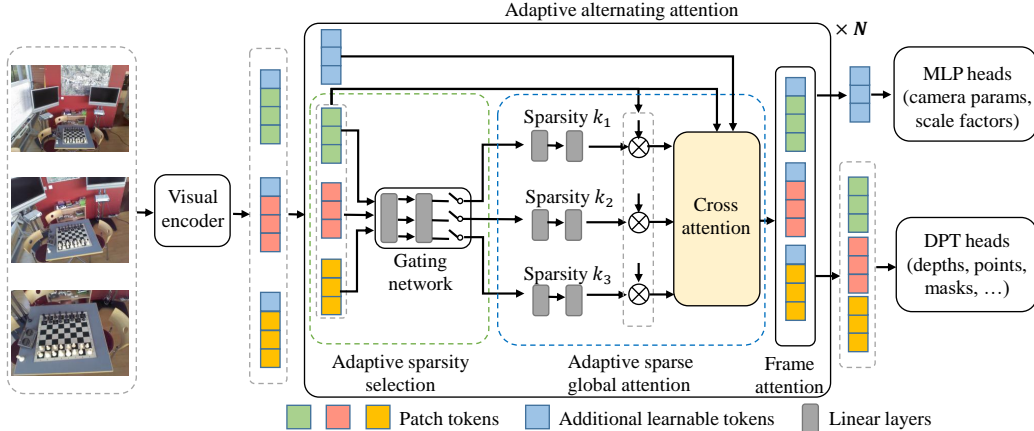


Figure 2: The overall framework of the proposed TurboVGGT.

geometric details within views. With the success of visual geometry transformers for multi-view 3D reconstruction, there have been some recent efforts employing token merging [33], block-sparse attention [38], subsampling global attention [35], and compressed descriptors [44] to accelerate visual geometry transformers. Our work belongs to this line of research, but unlike existing works, we propose to accelerate visual geometry transformers with adaptive alternating attention blocks.

3 Methodology

3.1 Approach Overview

An overview of the proposed TurboVGGT is depicted in Figure 2. The overall architecture of TurboVGGT consists of a visual encoder, N adaptive alternating attention blocks, and multiple task-specific prediction heads.

Visual Encoder. Given a sequence of L images $\{I_i\}_{i=1}^L$, we first employ a visual encoder (*e.g.*, DINOv2 [26]) to extract M patch tokens from each image, denoted as $\{x_{i,j}\}_{j=1}^M$, where $x_{i,j} \in \mathbb{R}^D$ is a D -dimensional patch token. In addition, following [39, 20], we also append additional learnable tokens, such as camera tokens and register tokens, to the sequence of patch tokens as the input to the subsequent modules.

Adaptive Alternating Attention Blocks. Next, we use N blocks of the proposed adaptive alternating attention to process the input token sequence. As shown in Figure 2, adaptive alternating attention consists of adaptive sparsity selection, adaptive sparse global attention, and frame attention. Specifically, in each block, we first aggregate the patch tokens for each frame and use a gating network to generate the gating score for each frame. Based on gating scores, we route the patch tokens of each frame to the branch corresponding to a specific sparsity ratio k_k and generate compressed representative tokens for each frame. Then, we perform cross-attention between the compressed tokens and the dense tokens to capture global correspondences across frames. After that, we perform frame attention for tokens from each frame to capture local geometric details within each frame. This process is repeated for N blocks.

Task-Specific Prediction Heads. Finally, we aggregate the output tokens from the adaptive alternating attention blocks and employ multiple task-specific prediction heads to decode the learned tokens into various 3D properties of each view. As shown in Figure 2, MLP heads [39, 20] are used to predict camera parameters and metric scaling factors, while DPT heads [29] are used to predict depth maps, point maps, confidence maps, *etc.*.

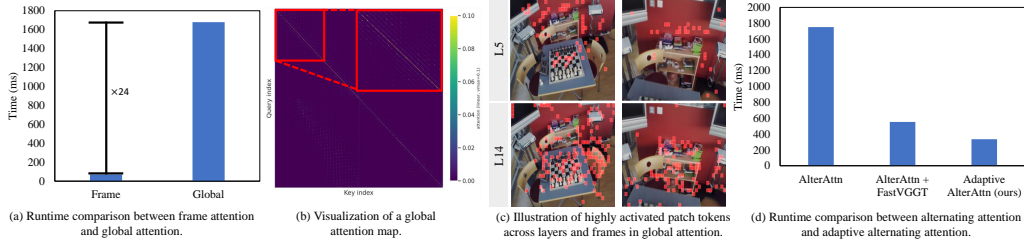


Figure 3: Motivation for our design. (a) The runtime comparison between a frame attention layer and a global attention layer during a single forward pass on 7-Scenes. (b) A visualization of an average global attention map in the alternating attention block. (c) An illustration of highly activated patch tokens (top 5% of activations across all frames) across layers and frames in global attention. (d) The runtime comparison between an alternating attention block and an adaptive alternating attention block during a single forward pass. Please refer to the supplementary material for enlarged visualizations.

3.2 Adaptive Alternating Attention

Adaptive Sparsity Selection. State-of-the-art visual geometry transformers [39, 20] typically employ alternating attention blocks consisting of frame-wise self-attention and cross-frame global full attention. This design allows transformers to learn local geometric details within each frame and to learn global correspondences across frames in an alternating manner. Although existing visual geometry transformers have achieved promising performance, they often suffer from long inference time and out-of-memory issues when processing long sequences. One of the main reasons is that global full attention involves dense global token interactions, which have a quadratic computational complexity with respect to the number of input tokens [33, 44, 35, 38]. As shown in Figure 3(a), a global attention layer consumes 24 times more runtime than a frame attention layer on the 7-Scenes dataset [34]. Consequently, as the number of input frames increases, the runtime of the global attention layer increases significantly compared to the frame attention layer. Nevertheless, as pointed out in prior work [38, 33], the attention map of each global attention layer is typically sparse (see Figure 3(b)), where only a small portion of patch tokens are highly activated for learning global relationships across frames while the majority of patch tokens have low attention activations. This suggests that it is not necessary to perform dense global full attention for all patch tokens across frames. However, unlike prior works that use the same sparsity ratio for all frames in all global attention layers, we further analyze the highly activated patch tokens across layers and frames in global attention. As shown in Figure 3(c), we find that the distribution of highly activated patch tokens can vary significantly across layers and frames. This indicates that the same sparsity ratio for all frames in all global attention layers may not be optimal. In light of this, we propose to adaptively select the sparsity level for each layer and frame rather than using a fixed sparsity ratio. Specifically, as shown in Figure 2, in each adaptive alternating attention block, we first aggregate the patch tokens for each frame. Then, we use a gating network consisting of an MLP to generate the gating score for each frame and route each frame to the branch corresponding to a specific sparsity ratio $k_k = \{k_1, k_2, \dots, k_n\}$. This is formulated as follows:

$$k_k = F_s(F_g(F_a(\{x_{i,j}\}_{j=1}^M))), \quad (1)$$

where $F_a(\cdot)$ is a function for generating frame-level representations, such as average pooling, $F_g(\cdot)$ is the gating network that generates the gating score for each frame, and $F_s(\cdot)$ is the softmax function that classifies each frame into one of the branches corresponding to a specific sparsity ratio k_k .

Adaptive Sparse Global Attention. Traditional multi-view 3D reconstruction methods [31, 32] typically capture global correspondences across frames by keypoint detection and matching rather than dense pixel-wise matching. This suggests that global dependencies across frames can be achieved by focusing on structurally informative regions, such as keypoints and edges. Moreover, as shown in Figure 3(c), highly activated patch tokens in global attention are sparsely distributed across frames and different frames may have different informative regions for learning global relationships. This further indicates that learning representative tokens for each frame as structurally informative regions can not only reduce computations of redundant tokens but also facilitate global geometry modeling across frames. In light of this, we propose to learn compressed representative tokens for each frame

and employ cross-attention between the compressed tokens and the dense tokens to capture global correspondences across frames. Specifically, in each branch corresponding to a specific sparsity ratio k_k , we employ an MLP $F_w(\cdot)$ to generate a weight matrix W_k for tokens of each frame, which is defined as:

$$W_i = F_w(x_i) + B_k, \quad (2)$$

where $x_i \in \mathbb{R}^{M \times D}$ are the patch tokens of frame i , $W_i \in \mathbb{R}^{M \times M_{k_k}}$ is the weight matrix, $M_{k_k} = \lfloor M(1 - k_k) \rfloor$ is the number of compressed representative tokens for the sparsity ratio k_k , and $B_k \in \mathbb{R}^{M \times M_{k_k}}$ is a learnable bias. Then, we generate the compressed representative tokens for each frame by aggregating the patch tokens of each frame using the weight matrix W_i as follows:

$$x_i^c = W_i^T x_i, \quad (3)$$

where $x_i^c \in \mathbb{R}^{M_{k_k} \times D}$ are the compressed representative tokens for frame i . Next, we concatenate the compressed representative tokens from all frames and additional learnable tokens (such as camera tokens and register tokens if used) as x^c . Here, if a reference frame is used, tokens of the reference frame are also concatenated. We then perform cross-attention between x^c and all dense tokens x' to capture global correspondences across frames, which is defined as follows:

$$x'' = \text{CrossAttn}(x'W^Q, x^cW^K, x^cW^V), \quad (4)$$

where x'' are the output dense tokens, W^Q , W^K , and W^V are the projection matrices for query, key, and value, respectively. In this way, we can capture global correspondences across frames while significantly reducing computational cost of global attention by using a small number of compressed representative tokens for each frame.

3.3 Model Optimization

Our TurboVGGT is trained in an end-to-end manner using a combination of losses for different prediction heads and a regularization term for the adaptive sparsity selection. The overall loss is:

$$\mathcal{L} = \mathcal{L}_{\text{recon}} + \lambda \mathcal{L}_{\text{reg}}, \quad (5)$$

where $\mathcal{L}_{\text{recon}}$ is a reconstruction loss, \mathcal{L}_{reg} is a sparsity regularization loss, and λ is a weight for the regularization term. Specifically, for the reconstruction loss $\mathcal{L}_{\text{recon}}$, we follow prior work [39, 43, 20] and use a sum of losses for different predictions, such as camera loss, depth loss, and pointmap loss, to supervise the learning of various 3D geometric properties. Please refer to [39, 43, 20] for the detailed definition of the reconstruction loss. For the sparsity regularization loss \mathcal{L}_{reg} , it is used to encourage the model to select larger sparsity levels for different layers and frames (thereby reducing the computational cost). By default, we use $\mathcal{L}_{\text{reg}} = \sum_{n=1}^N \sum_{i=1}^L (1 - k_k^{n,i})$, where $k_k^{n,i}$ is the sparsity ratio selected for frame i in the n -th adaptive alternating attention block. Additionally, we can add an entropy term to the sparsity regularization loss to push each frame in each layer to route decisively to a specific branch, which can be defined as $\sum_{n=1}^N (-\frac{1}{L} \sum_{i=1}^L p^{n,i} \log p^{n,i})$, where $p^{n,i}$ is the probability of selecting a specific branch for frame i in the n th block.

4 Experiments

4.1 Datasets and Experimental Setup

Datasets. We train our TurboVGGT on 13 high-quality datasets [20] spanning diverse indoor, outdoor, and in-the-wild scenes, including BlendedMVS [47], Mapillary Planet-Scale Depth [1], ScanNet++ v2 [48], Spring [25], TartanAirV2-WB [42, 52], UnrealStereo4K [36], Aria Synthetic Environments [2], DL3DV-10K [24], Dynamic Replica [19], MegaDepth [23], MVS-Synth [16], ParallelDomain-4D [37], and SAIL-VOS 3D [15]. We randomly resize and crop image sequences from these training datasets to various aspect ratios with a maximum resolution of 518 pixels. We evaluate our TurboVGGT on several challenging benchmark datasets, including 7-Scenes [34], N-RGBD [3], ScanNet-50 [7], RealEstate10K [53], and Sintel [5].

Evaluation Metrics. Following prior work [33], we evaluate our TurboVGGT on three tasks, including point cloud reconstruction, camera pose estimation, and depth estimation. For point cloud reconstruction, we report Accuracy (Acc, \downarrow), Completeness (Comp, \downarrow), and Normal Consistency

Table 1: Evaluation of point cloud reconstruction on 7-Scenes, N-RGBD, and ScanNet.

Method	7-Scenes - Stride 3								7-Scenes - Stride 10							
	Acc ↓		Comp ↓		NC ↑		Time ↓	Acc ↓		Comp ↓		NC ↑		Time ↓		
	Mean	Med.	Mean	Med.	Mean	Med.		Mean	Med.	Mean	Med.	Mean	Med.			
Fast3R [46]	0.045	0.027	0.047	0.010	0.616	0.627	43.7s	0.040	0.021	0.056	0.013	0.639	0.657	5.5s		
VGGT [39]	0.019	0.009	0.027	0.010	0.622	0.699	38.1s	0.019	0.008	0.027	0.010	0.628	0.710	4.5s		
SparseVGGT [38]	0.021	0.010	0.029	0.010	0.621	0.693	16.2s	0.020	0.010	0.028	0.010	0.629	0.707	2.6s		
AVGGT [35]	0.054	0.031	0.131	0.078	0.528	0.541	20.6s	-	-	-	-	-	-	-		
FastVGGT [33]	0.018	0.008	0.026	0.010	0.627	0.707	14.2s	0.018	0.008	0.027	0.010	0.632	0.717	2.7s		
TurboVGGT (ours)	0.016	0.009	0.026	0.010	0.639	0.714	9.6s	0.016	0.009	0.025	0.010	0.650	0.730	2.0s		

Method	N-RGBD - Stride 3								N-RGBD - Stride 10							
	Acc ↓		Comp ↓		NC ↑		Time ↓	Acc ↓		Comp ↓		NC ↑		Time ↓		
	Mean	Med.	Mean	Med.	Mean	Med.		Mean	Med.	Mean	Med.	Mean	Med.			
Fast3R [46]	0.074	0.036	0.024	0.011	0.658	0.682	68.9s	0.061	0.028	0.031	0.013	0.669	0.712	7.4s		
VGGT [39]	0.028	0.018	0.018	0.010	0.657	0.779	65.3s	0.016	0.010	0.016	0.009	0.669	0.791	7.2s		
SparseVGGT [38]	0.045	0.029	0.024	0.011	0.647	0.755	26.2s	0.041	0.027	0.027	0.012	0.652	0.763	4.1s		
FastVGGT [33]	0.031	0.020	0.019	0.010	0.662	0.788	30.2s	0.017	0.011	0.017	0.009	0.671	0.791	4.0s		
TurboVGGT (ours)	0.025	0.016	0.022	0.011	0.657	0.773	14.7s	0.021	0.014	0.021	0.011	0.664	0.783	2.9s		

Method	ScanNet - 500 Frames		ScanNet - 300 Frames		ScanNet - 100 Frames		Average	
	CD ↓	Time ↓	CD ↓	Time ↓	CD ↓	Time ↓	CD ↓	Time ↓
Fast3R [46]	0.701	97.3s	0.711	34.9s	0.723	4.8s	0.712	45.7s
VGGT [39]	0.464	90.1s	0.454	33.6s	0.438	4.9s	0.452	42.9s
SparseVGGT [38]	0.459	34.2s	0.453	14.2s	0.446	2.6s	0.453	17.0s
FastVGGT [33]	0.453	28.4s	0.447	12.3s	0.425	2.8s	0.442	14.5s
TurboVGGT (ours)	0.416	20.3s	0.413	9.5s	0.400	2.2s	0.410	10.7s

Table 2: Evaluation of camera pose estimation on 7-Scenes, N-RGBD, and RealEstate10K.

Method	7-Scenes				N-RGBD				RealEstate10K		
	RRA@30↑	RTA@30↑	AUC@30↑	Time ↓	RRA@30↑	RTA@30↑	AUC@30↑	Time ↓	RRA@30↑	RTA@30↑	AUC@30↑
Fast3R [46]	-	-	-	-	-	-	-	-	99.05	81.86	61.68
FLARE [51]	-	-	-	-	-	-	-	-	99.69	95.23	80.01
VGGT [39]	100.00	96.58	77.76	38.1s	100.00	99.47	91.59	65.3s	99.97	96.22	85.32
SparseVGGT [38]	100.00	93.40	70.07	16.2s	97.20	97.03	83.16	26.2s	99.61	91.35	76.65
AVGGT [35]	100.00	96.48	78.29	20.6s	-	-	-	-	99.93	95.62	85.45
Speed3R [30]	-	-	-	-	-	-	-	-	-	-	74.81
FlashVGGT [44]	-	-	-	-	-	-	-	-	99.92	95.61	85.30
FastVGGT [33]	99.99	96.29	76.90	14.2s	100.00	99.65	92.47	30.2s	99.92	94.76	84.37
TurboVGGT (ours)	100.00	96.83	81.87	9.6s	100.00	99.71	93.28	14.7s	99.93	94.69	84.31

(NC, ↑) on 7-Scenes and N-RGBD, and Chamfer Distance (CD, ↓) on ScanNet. For camera pose estimation, we report Relative Rotation Accuracy (RRA@30, ↑), Relative Translation Accuracy (RTA@30, ↑), and the Area Under the accuracy-threshold Curve for the minimum of RRA and RTA (AUC@30, ↑) on 7-Scenes, N-RGBD, and RealEstate10K. For depth estimation, we report Absolute Relative Error (AbsRel, ↓) and $\delta < 1.25$ ratio (↑) on 7-Scenes, N-RGBD, and Sintel. In addition, we also report inference time (seconds, ↓).

Implementation Details. We implement our TurboVGGT with Python and PyTorch. By default, we use VGGT [39] as the backbone and also adapt our approach to other backbones, *i.e.*, MapAnything [20] (denoted as TurboVGGT-M) and π^3 [43] (denoted as TurboVGGT- π), to validate the generalizability of our approach. We employ DINOv2 [26] as the visual encoder and build the adaptive alternating attention blocks as described in Sec. 3.2. For the adaptive sparsity selection, we use three branches and set $k_k = \{\frac{3}{4}, \frac{8}{9}, \frac{15}{16}\}$, *i.e.*, use three sparsity ratios of 75%, 89%, and 94% for the three branches, respectively. The number of the adaptive alternating attention blocks is determined by the backbone [39, 43, 20]. We construct the task-specific prediction heads following [39, 43, 20]. To facilitate model convergence, we initialize our TurboVGGT with pretrained weights from [39, 43, 20]. We train our TurboVGGT on 8 GPUs for 10 epochs using AdamW optimizer with a cosine annealing learning rate and a 1-epoch warm-up schedule. The maximum learning rate is set to 5×10^{-6} and decayed to 5×10^{-8} .

4.2 Comparison with State-of-the-Art Methods

Point Cloud Reconstruction. Table 1 shows results of point cloud reconstruction on 7-Scenes, N-RGBD, and ScanNet. Overall, our TurboVGGT achieves faster inference speed than state-of-the-art methods, while maintaining comparable or even better performance. Specifically, on 7-Scenes, our TurboVGGT outperforms state-of-the-art methods, such as FastVGGT [33], SparseVGGT [38], and AVGGT [35], in most metrics. Interestingly, TurboVGGT achieves overall better reconstruction quality than VGGT [39], while being 2-4× faster. This can be attributed to the adaptive sparse global

Table 3: Evaluation of depth estimation on 7-Scenes, N-RGBD, and Sintel.

Method	7-Scenes			N-RGBD			Sintel	
	AbsRel↓	$\delta < 1.25$ ↑	Time ↓	AbsRel↓	$\delta < 1.25$ ↑	Time ↓	AbsRel↓	$\delta < 1.25$ ↑
Fast3R [46]	-	-	-	-	-	-	0.544	0.509
FLARE [51]	-	-	-	-	-	-	0.606	0.402
VGGT [39]	0.264	0.958	38.1s	0.013	0.993	65.3s	0.335	0.599
SparseVGGT [38]	0.393	0.956	16.2s	0.015	0.990	26.2s	-	-
FlashVGGT [44]	-	-	-	-	-	-	0.346	0.586
FastVGGT [33]	0.394	0.953	14.2s	0.013	0.990	30.2s	0.337	0.582
TurboVGGT (ours)	0.296	0.980	9.6s	0.013	0.994	14.7s	0.287	0.650

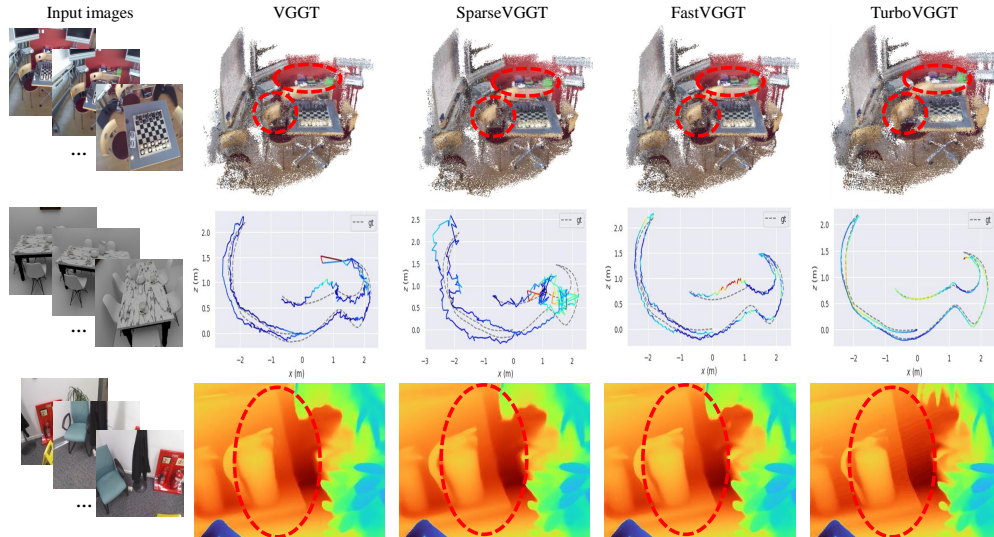


Figure 4: Qualitative comparison of point cloud reconstruction, camera pose estimation, and depth estimation. See supplementary materials for more qualitative results.

attention under the guidance of adaptive sparsity selection, which effectively captures global context while reducing redundant computations. On N-RGBD, our TurboVGGT also achieves competitive reconstruction performance while achieving faster inference than prior methods. Although the reconstruction quality of TurboVGGT is slightly inferior to FastVGGT in some metrics, TurboVGGT is $1.4\times$ faster than FastVGGT in the Stride 10 setting and $2.1\times$ faster in the Stride 3 setting. On ScanNet, TurboVGGT achieves the best reconstruction quality while being faster than prior methods. Figure 4 (first row) shows qualitative comparison of point cloud reconstruction. We can see that our TurboVGGT produces more complete point clouds compared with state-of-the-art methods.

Camera Pose Estimation. We report results of camera pose estimation on 7-Scenes (dense, stride=3), N-RGBD (dense), and RealEstate10K (sparse) in Table 2. On 7-Scenes and N-RGBD, our TurboVGGT achieves the best camera pose estimation performance and faster inference speed compared with state-of-the-art methods, such as FastVGGT [33], SparseVGGT [38], AVGGT [35], and VGGT [39]. In addition, we also evaluate TurboVGGT on RealEstate10K, which contains sparse image sequences. Our TurboVGGT still achieves competitive performance in this sparse setting. These results show the efficiency and effectiveness of our TurboVGGT in camera pose estimation across different settings. Figure 4 (second row) shows that the camera pose trajectory produced by our TurboVGGT is closer to the ground-truth trajectory than state-of-the-art competitors.

Depth Estimation. Table 3 shows results of depth estimation on 7-Scenes (dense), N-RGBD (dense), and Sintel (single). On 7-Scenes, our TurboVGGT achieves the second-best AbsRel and the best $\delta < 1.25$, while being faster than prior methods. On N-RGBD, our TurboVGGT achieves the best results in all metrics. Additionally, we evaluate TurboVGGT for monocular depth estimation on Sintel. Our TurboVGGT still achieves competitive performance in this monocular depth estimation setting, demonstrating the generalizability of our approach across settings. Figure 4 (third row) shows that our TurboVGGT produces higher-quality depth compared with state-of-the-art methods.

Table 4: Evaluation of our approach with various backbones on 7-Scenes.

Method	Point Cloud Estimation			Camera Pose Estimation			Depth Estimation		Time ↓
	Acc↓	Comp↓	NC↑	RRA@30↑	RTA@30↑	AUC@30↑	AbsRel↓	$\delta < 1.25$ ↑	
VGGT [39]	0.019	0.027	0.622	100.00	96.58	77.76	0.264	0.958	38.1s
TurboVGGT	0.016	0.026	0.639	100.00	96.83	81.87	0.296	0.980	9.6s
π^3 [43]	0.013	0.023	0.585	100.00	97.47	81.70	0.317	0.986	30.4s
TurboVGGT- π	0.014	0.024	0.585	100.00	97.11	80.81	0.331	0.983	6.2s
MapAnything [20]	0.018	0.024	0.579	100.00	92.45	70.29	0.314	0.975	15.3s
TurboVGGT-M	0.018	0.021	0.577	100.00	92.86	71.53	0.313	0.975	4.0s

Table 5: Ablation study of the proposed TurboVGGT on 7-Scenes.

Method	Ada. Selection		Ada. Global Attn		Acc↓	AUC@30↑	AbsRel↓
	Adaptive	Multi-branch	Weight matrix	Cross-attn			
V1	✗	✓	✓	✓	0.016	81.34	0.302
V2	✗	✗	✓	✓	0.016	80.88	0.300
V3	✓	✓	✗	✓	0.017	79.80	0.299
V4	✓	✓	✗	✗	0.047	65.73	0.311
Full	✓	✓	✓	✓	0.016	81.87	0.296

4.3 Adaptation to Different Backbones

To validate the generalizability of the proposed adaptive alternating attention, we adapt our TurboVGGT to more visual geometry transformer backbones, including π^3 [43] and MapAnything [20]. Results are shown in Table 4. We can see that our approach consistently improves the inference speed of these backbones while maintaining comparable or even better performance on point cloud reconstruction, camera pose estimation, and depth estimation. This demonstrates the effectiveness and generalizability of our adaptive alternating attention in accelerating visual geometry transformers across different backbones.

4.4 Ablation Study

We present the ablation study of our TurboVGGT on 7-Scenes in Table 5. For the adaptive sparsity selection, we report two variants of TurboVGGT, *i.e.*, V1 replaces the adaptive sparsity selection with fixed selection that evenly assigns frames to the three branches, and V2 removes the adaptive sparsity selection and uses only one branch with a fixed sparsity ratio. From Table 5, we can see that both V1 and V2 achieve worse performance than the full TurboVGGT. This shows the importance of the adaptive sparsity selection in routing frames to different branches for better capturing global context and reducing redundant computations. For the adaptive sparse global attention, we also report two variants of TurboVGGT, *i.e.*, V3 replaces weight matrix based compressed representative token learning with grid based token selection, and V4 removes the adaptive sparse global attention and uses global attention for merged tokens and upsampling to restore the original token number. From Table 5, we can see that without using weight matrix based compressed representative token learning, the reconstruction quality of V3 is worse than the full TurboVGGT. When removing the adaptive sparse global attention, V4 achieves significantly worse reconstruction quality than the full TurboVGGT. These results demonstrate the importance of the adaptive sparse global attention in learning representative tokens and performing global attention on these tokens for better capturing global relationships and reducing redundant computations.

5 Conclusion

In this work, we propose TurboVGGT for fast multi-view 3D reconstruction in a feed-forward manner. The core idea of TurboVGGT is to construct an efficient visual geometry transformer with adaptive alternating attention blocks, which consist of adaptive sparse global attention guided by adaptive sparsity selection for global geometry modeling and frame attention for local detail aggregation. Extensive experiments on multiple 3D reconstruction benchmarks demonstrate that TurboVGGT achieves a better balance between reconstruction quality and computational efficiency, outperforming state-of-the-art methods.

References

- [1] Manuel López Antequera, Pau Gargallo, Markus Hofinger, Samuel Rota Bulo, Yubin Kuang, and Peter Kotschieder. Mapillary planet-scale depth dataset. In *European Conference on Computer Vision*, pages 589–604. Springer, 2020.
- [2] Armen Avetisyan, Christopher Xie, Henry Howard-Jenkins, Tsun-Yi Yang, Samir Aroudj, Suvam Patra, Fuyang Zhang, Duncan Frost, Luke Holland, Campbell Orme, et al. Scene-script: Reconstructing scenes with an autoregressive structured language model. In *European Conference on Computer Vision*, pages 247–263. Springer, 2024.
- [3] Dejan Azinović, Ricardo Martin-Brualla, Dan B Goldman, Matthias Nießner, and Justus Thies. Neural rgb-d surface reconstruction. In *Proceedings of the IEEE/CVF conference on computer vision and pattern recognition*, pages 6290–6301, 2022.
- [4] Daniel Bolya, Cheng-Yang Fu, Xiaoliang Dai, Peizhao Zhang, Christoph Feichtenhofer, and Judy Hoffman. Token merging: Your vit but faster. In *The Eleventh International Conference on Learning Representations*, 2023.
- [5] Daniel J Butler, Jonas Wulff, Garrett B Stanley, and Michael J Black. A naturalistic open source movie for optical flow evaluation. In *European conference on computer vision*, pages 611–625. Springer, 2012.
- [6] Xingyu Chen, Yue Chen, Yuliang Xiu, Andreas Geiger, and Anpei Chen. TTT3r: 3d reconstruction as test-time training. In *The Fourteenth International Conference on Learning Representations*, 2026.
- [7] Angela Dai, Angel X Chang, Manolis Savva, Maciej Halber, Thomas Funkhouser, and Matthias Nießner. Scannet: Richly-annotated 3d reconstructions of indoor scenes. In *Proceedings of the IEEE conference on computer vision and pattern recognition*, pages 5828–5839, 2017.
- [8] Tri Dao. Flashattention-2: Faster attention with better parallelism and work partitioning. *arXiv preprint arXiv:2307.08691*, 2023.
- [9] Tri Dao, Dan Fu, Stefano Ermon, Atri Rudra, and Christopher Ré. Flashattention: Fast and memory-efficient exact attention with io-awareness. *Advances in neural information processing systems*, 35:16344–16359, 2022.
- [10] Alexey Dosovitskiy, Lucas Beyer, Alexander Kolesnikov, Dirk Weissenborn, Xiaohua Zhai, Thomas Unterthiner, Mostafa Dehghani, Matthias Minderer, Georg Heigold, Sylvain Gelly, Jakob Uszkoreit, and Neil Houlsby. An image is worth 16x16 words: Transformers for image recognition at scale. In *International Conference on Learning Representations*, 2021.
- [11] Sven Elfle, Ruilong Li, Sérgio Agostinho, Zan Gojcic, Laura Leal-Taixé, Qunjie Zhou, and Aljosa Osep. Vgg-t³: Offline feed-forward 3d reconstruction at scale. *arXiv preprint arXiv:2602.23361*, 2026.
- [12] Yasutaka Furukawa and Carlos Hernández. Multi-view stereo: A tutorial. *Foundations and Trends in Computer Graphics and Vision*, 9(1-2):1–148, 2015.
- [13] Dongchen Han, Tianzhu Ye, Yizeng Han, Zhuofan Xia, Siyuan Pan, Pengfei Wan, Shiji Song, and Gao Huang. Agent attention: On the integration of softmax and linear attention. In *European conference on computer vision*, pages 124–140. Springer, 2024.
- [14] Jisang Han, Honggyu An, Jaewoo Jung, Takuya Narihira, Junyoung Seo, Kazumi Fukuda, Chaehyun Kim, Sunghwan Hong, Yuki Mitsufuji, and Seungryong Kim. Enhancing 3d reconstruction for dynamic scenes. In *The Thirty-ninth Annual Conference on Neural Information Processing Systems*, 2025.
- [15] Yuan-Ting Hu, Jiahong Wang, Raymond A Yeh, and Alexander G Schwing. Sail-vos 3d: A synthetic dataset and baselines for object detection and 3d mesh reconstruction from video data. In *Proceedings of the IEEE/CVF Conference on Computer Vision and Pattern Recognition*, pages 1418–1428, 2021.
- [16] Po-Han Huang, Kevin Matzen, Johannes Kopf, Narendra Ahuja, and Jia-Bin Huang. Deepmvs: Learning multi-view stereopsis. In *Proceedings of the IEEE conference on computer vision and pattern recognition*, pages 2821–2830, 2018.
- [17] Andrew Jaegle, Felix Gimeno, Andy Brock, Oriol Vinyals, Andrew Zisserman, and Joao Carreira. Perceiver: General perception with iterative attention. In *International conference on machine learning*, pages 4651–4664. PMLR, 2021.

- [18] Haiyan Jin, Rundi Wu, Tianyuan Zhang, Ruiqi Gao, Jonathan T Barron, Noah Snavely, and Aleksander Holynski. Zipmap: Linear-time stateful 3d reconstruction via test-time training. *arXiv preprint arXiv:2603.04385*, 2026.
- [19] Nikita Karaev, Ignacio Rocco, Benjamin Graham, Natalia Neverova, Andrea Vedaldi, and Christian Rupprecht. Dynamicstereo: Consistent dynamic depth from stereo videos. In *Proceedings of the IEEE/CVF Conference on Computer Vision and Pattern Recognition*, pages 13229–13239, 2023.
- [20] Nikhil Varma Keetha, Norman Müller, Johannes Schönberger, Lorenzo Porzi, Yuchen Zhang, Tobias Fischer, Arno Knapitsch, Duncan Zauss, Ethan Weber, Nelson Antunes, Jonathon Luiten, Manuel Lopez-Antequera, Samuel Rota Bulò, Christian Richardt, Deva Ramanan, Sebastian Scherer, and Peter Kotschieder. Mapanything: Universal feed-forward metric 3d reconstruction. In *Thirteenth International Conference on 3D Vision*, 2026.
- [21] Vincent Leroy, Yohann Cabon, and Jérôme Revaud. Grounding image matching in 3d with mast3r. In *European conference on computer vision*, pages 71–91. Springer, 2024.
- [22] Junnan Li, Dongxu Li, Silvio Savarese, and Steven Hoi. Blip-2: Bootstrapping language-image pre-training with frozen image encoders and large language models. In *International conference on machine learning*, pages 19730–19742. PMLR, 2023.
- [23] Zhengqi Li and Noah Snavely. Megadepth: Learning single-view depth prediction from internet photos. In *Proceedings of the IEEE conference on computer vision and pattern recognition*, pages 2041–2050, 2018.
- [24] Lu Ling, Yichen Sheng, Zhi Tu, Wentian Zhao, Cheng Xin, Kun Wan, Lantao Yu, Qianyu Guo, Zixun Yu, Yawen Lu, et al. D13dv-10k: A large-scale scene dataset for deep learning-based 3d vision. In *Proceedings of the IEEE/CVF Conference on Computer Vision and Pattern Recognition*, pages 22160–22169, 2024.
- [25] Lukas Mehl, Jenny Schmalfluss, Azin Jahedi, Yaroslava Nalivayko, and Andrés Bruhn. Spring: A high-resolution high-detail dataset and benchmark for scene flow, optical flow and stereo. In *Proceedings of the IEEE/CVF Conference on Computer Vision and Pattern Recognition*, pages 4981–4991, 2023.
- [26] Maxime Oquab, Timothée Darcet, Théo Moutakanni, Huy Vo, Marc Szafraniec, Vasil Khalidov, Pierre Fernandez, Daniel Haziza, Francisco Massa, Alaaeldin El-Nouby, et al. Dinov2: Learning robust visual features without supervision. *Transactions on Machine Learning Research Journal*, 2024.
- [27] Emanuele Palazzolo, Jens Behley, Philipp Lottes, Philippe Giguere, and Cyrill Stachniss. Refusion: 3d reconstruction in dynamic environments for rgb-d cameras exploiting residuals. In *2019 IEEE/RSJ International Conference on Intelligent Robots and Systems*, pages 7855–7862. IEEE, 2019.
- [28] Linfei Pan, Dániel Baráth, Marc Pollefeys, and Johannes L Schönberger. Global structure-from-motion revisited. In *European Conference on Computer Vision*, pages 58–77. Springer, 2024.
- [29] René Ranftl, Alexey Bochkovskiy, and Vladlen Koltun. Vision transformers for dense prediction. In *Proceedings of the IEEE/CVF international conference on computer vision*, pages 12179–12188, 2021.
- [30] Weining Ren, Xiao Tan, and Kai Han. Speed3r: Sparse feed-forward 3d reconstruction models. *arXiv preprint arXiv:2603.08055*, 2026.
- [31] Johannes L Schonberger and Jan-Michael Frahm. Structure-from-motion revisited. In *Proceedings of the IEEE conference on computer vision and pattern recognition*, pages 4104–4113, 2016.
- [32] Johannes L Schönberger, Enliang Zheng, Jan-Michael Frahm, and Marc Pollefeys. Pixelwise view selection for unstructured multi-view stereo. In *European conference on computer vision*, pages 501–518. Springer, 2016.
- [33] You Shen, Zhipeng Zhang, Yansong Qu, Xiawu Zheng, Jiayi Ji, Shengchuan Zhang, and Liujuan Cao. FastVGGT: Fast visual geometry transformer. In *The Fourteenth International Conference on Learning Representations*, 2026.

- [34] Jamie Shotton, Ben Glocker, Christopher Zach, Shahram Izadi, Antonio Criminisi, and Andrew Fitzgibbon. Scene coordinate regression forests for camera relocalization in rgb-d images. In *Proceedings of the IEEE conference on computer vision and pattern recognition*, pages 2930–2937, 2013.
- [35] Xianbing Sun, Zhikai Zhu, Zhengyu Lou, Bo Yang, Jinyang Tang, Liqing Zhang, He Wang, and Jianfu Zhang. Avggt: Rethinking global attention for accelerating vgg. *arXiv preprint arXiv:2512.02541*, 2025.
- [36] Fabio Tosi, Yiyi Liao, Carolin Schmitt, and Andreas Geiger. Smd-nets: Stereo mixture density networks. In *Proceedings of the IEEE/CVF conference on computer vision and pattern recognition*, pages 8942–8952, 2021.
- [37] Basile Van Hoorick, Rundi Wu, Ege Ozguroglu, Kyle Sargent, Ruoshi Liu, Pavel Tokmakov, Achal Dave, Changxi Zheng, and Carl Vondrick. Generative camera dolly: Extreme monocular dynamic novel view synthesis. In *European Conference on Computer Vision*, pages 313–331. Springer, 2024.
- [38] Chung-Shien Brian Wang, Christian Schmidt, Jens Piekenbrinck, and Bastian Leibe. Faster vgg with block-sparse global attention. *arXiv preprint arXiv:2509.07120*, 2025.
- [39] Jianyuan Wang, Minghao Chen, Nikita Karaev, Andrea Vedaldi, Christian Rupprecht, and David Novotny. Vgg: Visual geometry grounded transformer. In *Proceedings of the Computer Vision and Pattern Recognition Conference*, pages 5294–5306, 2025.
- [40] Qianqian Wang, Yifei Zhang, Aleksander Holynski, Alexei A Efros, and Angjoo Kanazawa. Continuous 3d perception model with persistent state. In *Proceedings of the Computer Vision and Pattern Recognition Conference*, pages 10510–10522, 2025.
- [41] Shuzhe Wang, Vincent Leroy, Yohann Cabon, Boris Chidlovskii, and Jerome Revaud. Dust3r: Geometric 3d vision made easy. In *Proceedings of the IEEE/CVF conference on computer vision and pattern recognition*, pages 20697–20709, 2024.
- [42] Wenshan Wang, Delong Zhu, Xiangwei Wang, Yaoyu Hu, Yuheng Qiu, Chen Wang, Yafei Hu, Ashish Kapoor, and Sebastian Scherer. Tartanair: A dataset to push the limits of visual slam. In *2020 IEEE/RSJ International Conference on Intelligent Robots and Systems (IROS)*, pages 4909–4916. IEEE, 2020.
- [43] Yifan Wang, Jianjun Zhou, Haoyi Zhu, Wenzheng Chang, Yang Zhou, Zizun Li, Junyi Chen, Jiangmiao Pang, Chunhua Shen, and Tong He. π^3 : Scalable permutation-equivariant visual geometry learning. *arXiv e-prints*, pages arXiv–2507, 2025.
- [44] Zipeng Wang and Dan Xu. Flashvgg: Efficient and scalable visual geometry transformers with compressed descriptor attention. *arXiv preprint arXiv:2512.01540*, 2025.
- [45] Cong Wei, Brendan Duke, Ruwei Jiang, Parham Aarabi, Graham W Taylor, and Florian Shkurti. Sparsifiner: Learning sparse instance-dependent attention for efficient vision transformers. In *Proceedings of the IEEE/CVF Conference on Computer Vision and Pattern Recognition*, pages 22680–22689, 2023.
- [46] Jianing Yang, Alexander Sax, Kevin J Liang, Mikael Henaff, Hao Tang, Ang Cao, Joyce Chai, Franziska Meier, and Matt Feiszli. Fast3r: Towards 3d reconstruction of 1000+ images in one forward pass. In *Proceedings of the Computer Vision and Pattern Recognition Conference*, pages 21924–21935, 2025.
- [47] Yao Yao, Zixin Luo, Shiwei Li, Jingyang Zhang, Yufan Ren, Lei Zhou, Tian Fang, and Long Quan. Blendedmvs: A large-scale dataset for generalized multi-view stereo networks. In *Proceedings of the IEEE/CVF conference on computer vision and pattern recognition*, pages 1790–1799, 2020.
- [48] Chandan Yeshwanth, Yueh-Cheng Liu, Matthias Nießner, and Angela Dai. Scannet++: A high-fidelity dataset of 3d indoor scenes. In *Proceedings of the IEEE/CVF International Conference on Computer Vision*, pages 12–22, 2023.
- [49] Wang Zeng, Sheng Jin, Wentao Liu, Chen Qian, Ping Luo, Wanli Ouyang, and Xiaogang Wang. Not all tokens are equal: Human-centric visual analysis via token clustering transformer. In *Proceedings of the IEEE/CVF conference on computer vision and pattern recognition*, pages 11101–11111, 2022.

- [50] Jintao Zhang, Chendong Xiang, Haofeng Huang, Jia Wei, Haocheng Xi, Jun Zhu, and Jianfei Chen. Spargeattention: Accurate and training-free sparse attention accelerating any model inference. In *International Conference on Machine Learning*, pages 76397–76413. PMLR, 2025.
- [51] Shangzhan Zhang, Jianyuan Wang, Yinghao Xu, Nan Xue, Christian Rupprecht, Xiaowei Zhou, Yujun Shen, and Gordon Wetzstein. Flare: Feed-forward geometry, appearance and camera estimation from uncalibrated sparse views. In *Proceedings of the Computer Vision and Pattern Recognition Conference*, pages 21936–21947, 2025.
- [52] Yuchen Zhang, Nikhil Keetha, Chenwei Lyu, Bhuvan Jhamb, Yutian Chen, Yuheng Qiu, Jay Karhade, Shreyas Jha, Yaoyu Hu, Deva Ramanan, et al. Ufm: A simple path towards unified dense correspondence with flow. *arXiv preprint arXiv:2506.09278*, 2025.
- [53] Tinghui Zhou, Richard Tucker, John Flynn, Graham Fyffe, and Noah Snavely. Stereo magnification: learning view synthesis using multiplane images. *ACM Transactions on Graphics (TOG)*, 37(4):1–12, 2018.
- [54] Dong Zhuo, Wenzhao Zheng, Jiahe Guo, Yuqi Wu, Jie Zhou, and Jiwen Lu. Streaming visual geometry transformer. In *The Fourteenth International Conference on Learning Representations*, 2026.

A Technical appendices and supplementary material

A.1 Limitation and Future Work

While the proposed TurboVGGT achieves superior performance on fast multi-view 3D reconstruction, there are still some limitations that can be addressed in future work. First, TurboVGGT does not explicitly model temporal dynamics of input sequences, which may limit its performance on highly dynamic scenes. Second, although TurboVGGT achieves a balance between reconstruction quality and computational efficiency, there is still room for improvement, especially for challenging scenes with complex geometry. In future work, we aim to explore more effective ways to model temporal dynamics for 4D reconstruction and improve the model architecture design of TurboVGGT for better performance.

A.2 Societal Impacts

This work presents an efficient visual geometry transformer for multi-view 3D reconstruction, which can potentially benefit various applications such as virtual reality, robotics, and autonomous driving. We do not discover direct negative societal impacts of our approach. However, since our approach requires training with large-scale datasets and substantial computational resources, it may raise concerns regarding data privacy and environmental impact. These societal impacts should be carefully considered when using our approach in real-world applications.

A.3 Complexity Analysis of Adaptive Sparse Global Attention

As discussed in the main paper, global full attention used in conventional visual geometry transformers [39] is computationally expensive and can lead to long inference time and out-of-memory issues when processing long sequences. The computational complexity of global full attention is $\mathcal{O}(L^2M^2)$, which is quadratic with respect to the number of input tokens, where L is the number of input frames and M is the number of patch tokens for each frame. For our adaptive sparse global attention, the computational cost mainly comes from the cross-attention between the compressed representative tokens and the dense tokens, while the other operations have relatively less computational cost (especially for long sequences) which can be ignored for simplicity. Specifically, the computational complexity of our adaptive sparse global attention is $\mathcal{O}(L^2M^2(1 - k_k))$, where k_k is the sparsity ratio. Since we encourage our model to select a large sparsity ratio k_k for each frame and have $(1 - k_k) \ll 1$, e.g., $(1 - k_k) = \{25\%, 11\%, 6\%\}$, our adaptive sparse global attention significantly reduces the computational complexity compared to global full attention, which is consistent with the significant runtime reduction observed in our experiments (see Section 4). Although some existing works [33, 44] also have a computational complexity similar to ours, they typically use the same sparsity ratio for all frames across layers and lack mechanisms to adaptively learn representative

tokens that can effectively capture global relationships; in contrast, our method adaptively selects the sparsity level across layers and frames and achieves better reconstruction quality while maintaining fast inference speed.

A.4 Memory Efficiency Analysis

In Table 6, we compare the peak GPU memory usage of our TurboVGGT, VGGT [39], SparseVGGT [38], and FastVGGT [33] on 7-Scenes (dense setting). We can see that our TurboVGGT not only achieves faster inference speed but also reduces the peak GPU memory usage compared with these state-of-the-art methods. This result further shows the superiority of our TurboVGGT that can effectively reduce the computational cost and memory usage for multi-view 3D reconstruction.

Table 6: Memory efficiency analysis on 7-Scenes.

Metrics	VGGT [39]	SparseVGGT [38]	FastVGGT [33]	TurboVGGT (Ours)
Peak inference memory↓	25.24 GB	27.84 GB	31.18 GB	23.47 GB
Inference speed↑	8.27 FPS	19.56 FPS	22.16 FPS	33.01 FPS

A.5 Evaluation of Video Depth Estimation

In Table 7, we further perform evaluation of video depth estimation on Sintel [5] and Bonn [27], following [11]. We can see that our TurboVGGT achieves the best performance on both datasets, outperforming state-of-the-art methods such as VGG-T³ [11] and ZipMap [18]. This further demonstrates the superior performance of our TurboVGGT in video depth estimation, which is crucial for multi-view 3D reconstruction.

Table 7: Evaluation of video depth estimation on Sintel and Bonn. Results of some methods are taken from [11, 18].

Datasets	Metrics	VGGT [39]	SparseVGGT [38]	FastVGGT [33]	TTT3R [6]	ZipMap [18]	VGG-T ³ [11]	TurboVGGT (Ours)
Sintel	AbsRel↓	0.300	0.304	0.307	0.469	0.248	0.345	0.212
	$\delta < 1.25$ ↑	0.646	0.639	0.630	0.510	0.695	0.581	0.716
Bonn	AbsRel↓	0.059	0.057	0.058	0.061	0.059	0.063	0.053
	$\delta < 1.25$ ↑	0.967	0.968	0.969	0.969	0.973	0.963	0.975

A.6 Impact of Sparsity Regularization Loss \mathcal{L}_{reg}

In Table 8, we analyze the impact of the sparsity regularization loss \mathcal{L}_{reg} on our TurboVGGT. When setting $\lambda_{reg} = 0$, our TurboVGGT does not have an explicit regularization to encourage sparsity, resulting in both worse reconstruction quality and slower inference speed compared with our full model. When setting $\lambda_{reg} = 0.001$, the inference speed is improved compared with $\lambda_{reg} = 0$, but the reconstruction quality is still worse than our full model. When setting $\lambda_{reg} = 0.01$, our TurboVGGT achieves the best performance in terms of both reconstruction quality and inference speed.

Table 8: Impact of sparsity regularization loss \mathcal{L}_{reg} (on 7-Scenes).

Method	Acc↓	AUC@30↑	AbsRel↓	Time↓
TurboVGGT w/o regularization loss ($\lambda_{reg} = 0$)	0.016	80.63	0.309	14.5s
TurboVGGT ($\lambda_{reg} = 0.001$)	0.017	80.23	0.301	12.5s
TurboVGGT (default, $\lambda_{reg} = 0.01$)	0.016	81.87	0.296	9.6s

A.7 Impact of Separating Additional Learnable Tokens

In our design, we separate additional learnable tokens of each frame from dense patch tokens during adaptive sparsity selection and compressed representative token learning. This allows our model to focus on capturing global relationships across frames without being distracted by additional global tokens. In Table 9, we report a variant of our TurboVGGT that does not separate the additional

learnable tokens during adaptive sparsity selection and compressed representative token learning. It can be seen that this variant performs slightly worse than our full model for multi-view 3D reconstruction.

Table 9: Impact of separating additional learnable tokens (on 7-Scenes).

Method	Acc↓	Comp↓	RRA@30↑	RTA@30↑	AbsRel↓	$\delta < 1.25$ ↑
TurboVGGT	0.016	0.026	100.00	96.83	0.296	0.980
TurboVGGT w/o separating additional tokens	0.017	0.024	100.00	96.29	0.314	0.979

A.8 Difference from Q-Former and Perceiver

Q-Former [22] and Perceiver [17] employ a compact set of latent queries and cross-attention to perform attention over the input in a low-rank latent space, which shares some merits with our adaptive sparse global attention design. However, our approach significantly differs from them in motivation and design. Q-Former and Perceiver use a set of learnable latents for all inputs to transform the inputs into a compact latent space, which may not be optimal for multi-view 3D reconstruction where the importance of different frames can vary significantly; in contrast, our approach adaptively selects the sparsity level across layers and frames and learns compressed representative tokens for each frame. More importantly, our method is specifically designed for multi-view 3D reconstruction, which requires modeling global correspondences across frames while preserving local geometric details within each frame; in contrast, Q-Former and Perceiver are designed for general language and computer vision tasks and do not explicitly consider the unique challenges of multi-view 3D reconstruction. As shown Table 10, we report a variant of VGGT that uses a set of learnable query latents. We can see that this variant achieves significantly worse reconstruction quality compared with our TurboVGGT. This result further demonstrates the importance of our adaptive sparse global attention in TurboVGGT for achieving superior performance, while using existing design such as learnable query latents is not sufficient to capture representative tokens across frames for multi-view 3D reconstruction.

Table 10: Comparison between the proposed design and a variant of VGGT that uses learnable query latents (point cloud reconstruction on 7-Scenes).

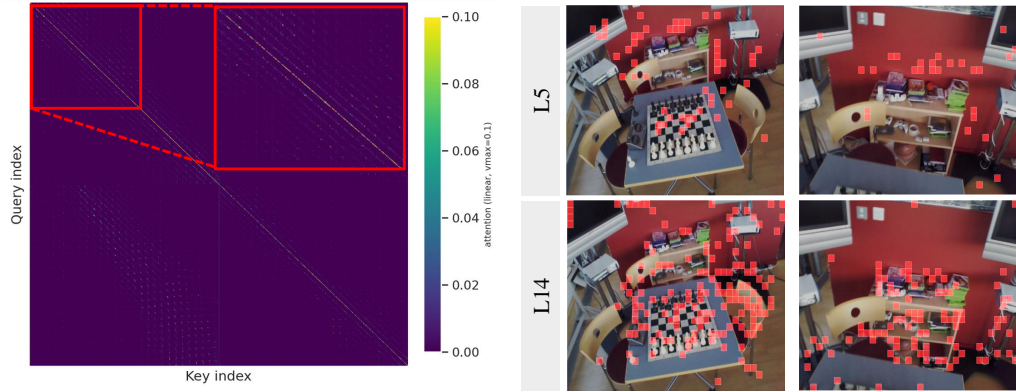
Method	Acc↓	Comp↓	RRA@30↑	RTA@30↑	AbsRel↓	$\delta < 1.25$ ↑
TurboVGGT	0.016	0.026	100.00	96.83	0.296	0.980
VGGT + learnable query latents	0.109	0.041	91.05	78.24	0.362	0.975

A.9 Supplementary Visualization

In Figure 5, we provide supplementary visualizations of the motivation for our proposed adaptive alternating attention, which are enlarged visualizations of Figure 3 in the main paper.

A.10 More Qualitative Results

In Figures 6, 7, and 8, we provide more qualitative results of point cloud reconstruction, camera pose estimation, and depth estimation. From these results, we can see that our TurboVGGT can effectively reconstruct point clouds, estimate camera poses, and predict depth maps. These results further demonstrate the superior performance of our TurboVGGT compared with state-of-the-art methods.



(a) Visualization of a global attention map.

(b) Illustration of highly activated patch tokens across frames in global attention.

Figure 5: Supplementary visualization of the motivation for the proposed adaptive alternating attention (Enlarged visualizations). (a) A visualization of an average global attention map in the alternating attention block. (b) An illustration of highly activated patch tokens of different frames in global attention.

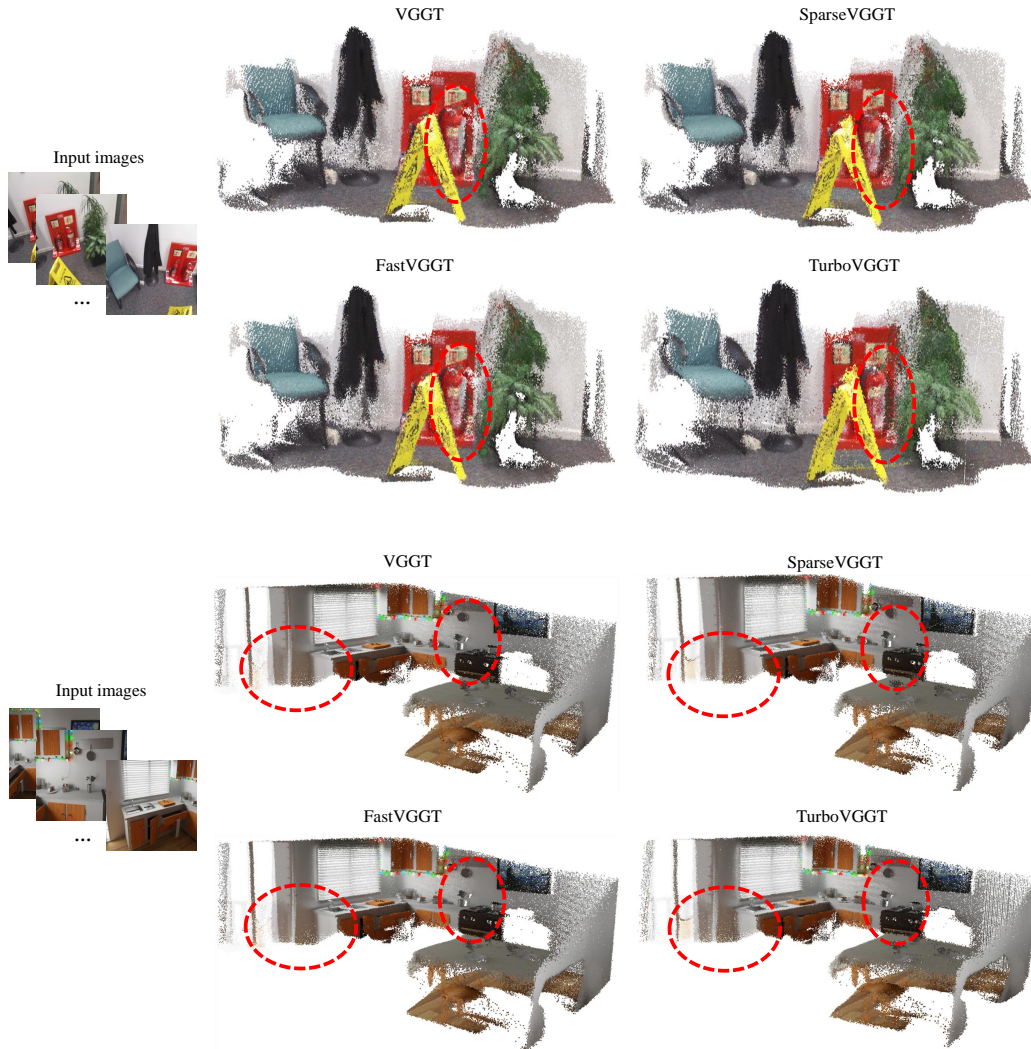


Figure 6: Qualitative comparison of point cloud reconstruction.

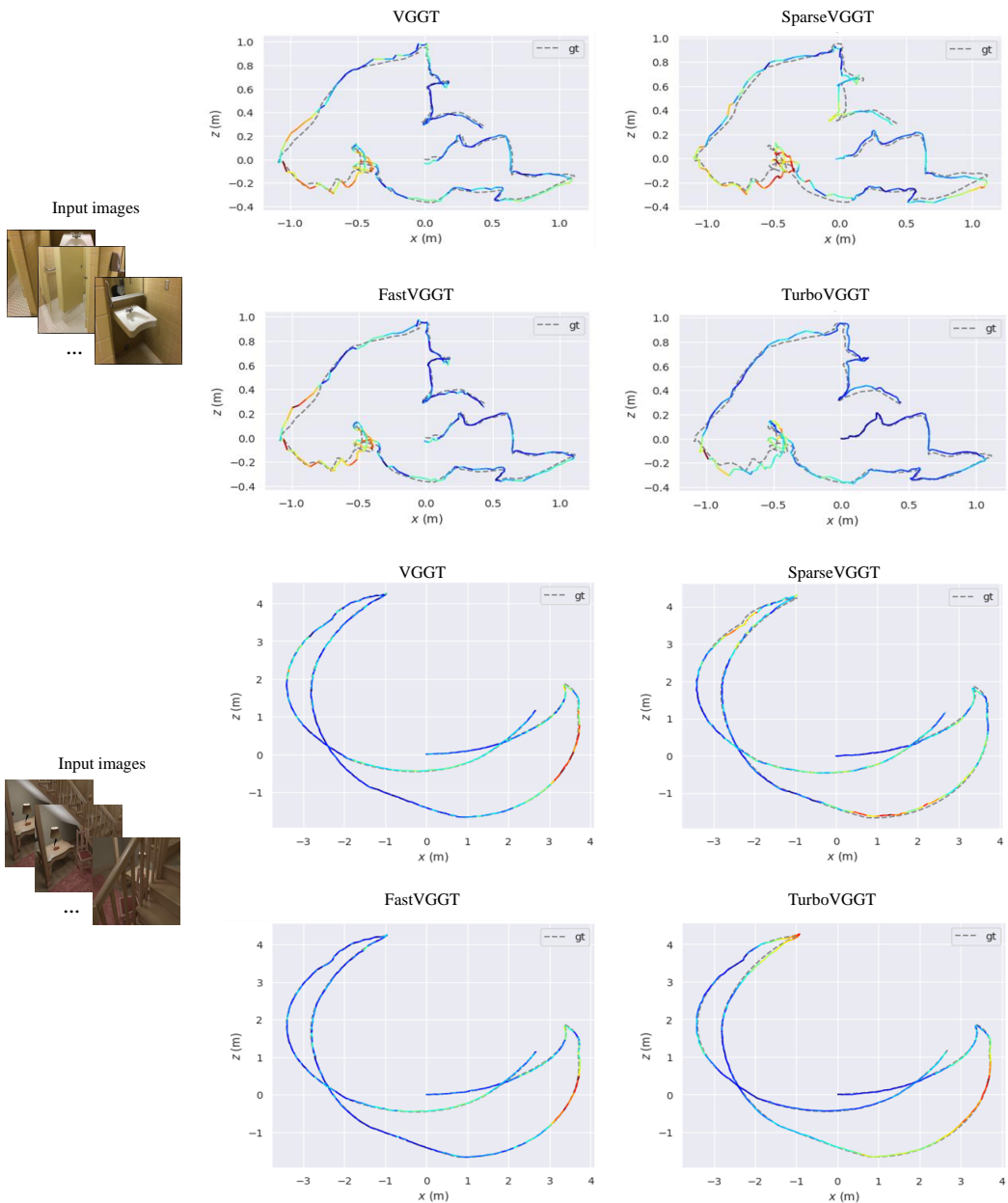


Figure 7: Qualitative comparison of camera pose estimation.

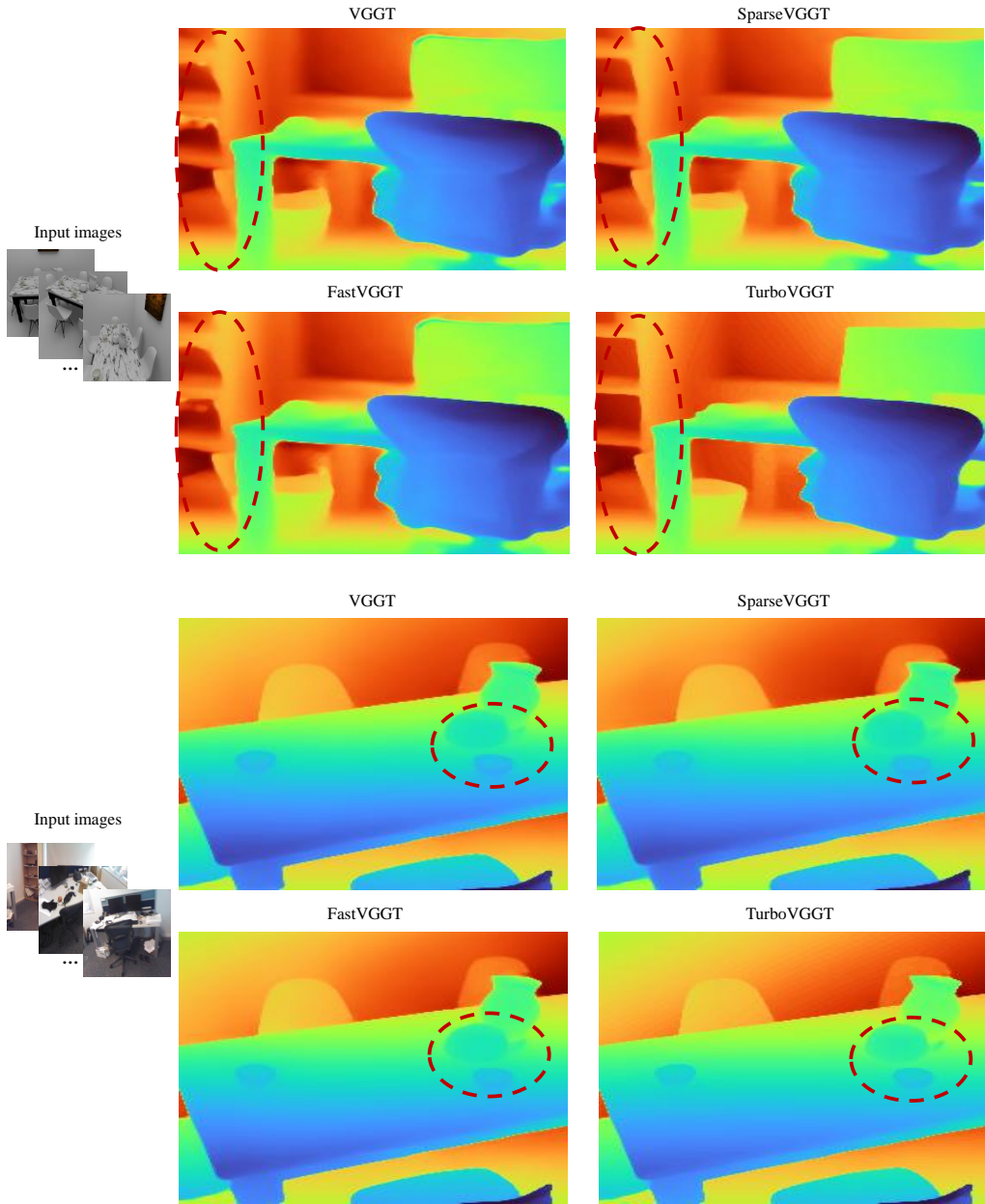


Figure 8: Qualitative comparison of depth estimation.